SLAC–PUB–4977
LBL–27160
May 1989
(A/E)

MEASURING THE MASS AND WIDTH OF THE Z^0: THE STATUS OF THE ENERGY SPECTROMETERS*

F. ROUSE§ AND M. LEVI
Lawrence Berkeley Laboratory, Berkeley, CA, 94720 USA

J. KENT, M. KING, C. VON ZANTHIER, AND S. WATSON
University of California at Santa Cruz, Santa Cruz, CA, 95064 USA

P. BAMBADE,‡ R. ERICKSON, C. K. JUNG, J. NASH, AND G. WORMSER‡
Stanford Linear Accelerator Center, Stanford University, Stanford, CA, 94309 USA

ABSTRACT

The Stanford Linear Collider (SLC) located at the Stanford Linear Accelerator Center (SLAC) collides electrons and positrons produced in the linear accelerator pulse by pulse. The object is to produce collisions energetic enough to produce the heavy intermediate vector boson, the Z^0. An essential component of the SLC physics program is the precise knowledge of the center-of-mass energy of each interaction. We measure the energy of each collision by using two energy spectrometers. The spectrometers are located in extraction lines of each beam. We will measure the energy of each beam to 20 MeV or 5 parts in 10^4. We report here on the status of the energy spectrometer system.

Contributed to the Symposium on the 4th Family of Quarks and Leptons, Santa Monica, CA, February 23–25, 1989

* Work supported by the U.S. Department of Energy, contracts DE–AC03–76SF00098, DE–AC03–76SF00515, and DE–AC03–76SF00010.

§ Presidential Fellow, University of California at Berkeley, CA 94720 USA.

‡ Present address: LAL–Orsay, 91405 France.

INTRODUCTION

The SLAC Linear Collider (SLC) is a novel electron–positron accelerator designed to produce center-of-mass energies of around 93 GeV, the mass of the Z^0 particle. The collisions are between electrons and positrons produced directly by the accelerator. Previously, energetic electron–positron collisions were produced by counter-rotating beams of electrons and positrons stored in a storage ring. The beams are discarded, pulse by pulse, at the SLC. They are directed into a beam dump after the interaction point (IP).

We will measure the mass of the Z^0 by measuring the energy of the beams before they are steered into the beam dump. We measure the energy of the two beams pulse by pulse. We will then make a luminosity-weighted histogram of the number of Z^0 particles detected as a function of the measured sum of the two beam energies. We can also use this technique to measure the Z^0 line shape and therefore determine the width of the Z^0.

The measurements of the mass and the width are important because they are indirect tests of the Standard Model of the electroweak interaction. The cross section for the process

$$e^+e^- \rightarrow Z^0 \rightarrow f\bar{f}$$

is given by[1,2]:

$$\sigma = \frac{12\pi\, s}{{m_Z}^2} \frac{\Gamma(Z^0 \rightarrow e^+e^-)\,\Gamma(Z^0 \rightarrow f\bar{f})}{(s-m_Z^2)^2 + \Gamma_T m_Z^2} \quad , \tag{1}$$

where s is the center-of-mass energy of the interaction squared, Z^0 is the mass of the Z^0, Γ_T is the total width of the Z^0, and $\Gamma(Z^0 \rightarrow f\bar{f})$ is the width of this particular decay mode of the Z. This expression simplifies when the center-of-mass energy of the interaction equals the mass of the Z^0 to

$$\sigma = \frac{12\pi}{m_Z^2 s} \frac{\Gamma_{e^+e^-}\Gamma_{f\bar{f}}}{\Gamma_T} \quad . \tag{2}$$

We can express the expected widths of the decay of the Z^0 in terms of the couplings of leptons and quarks to the Z^0 fields[1,2]:

$$\Gamma_{f\bar{f}} = \frac{G_F {m_z}^2}{24\pi\sqrt{2}} K_f F_{QCD}(v_f^2 + a_f^2) \quad , \tag{3}$$

where f is the final state, G_F is the Fermi constant, K_f is the radiative correction to decay, F_{QCD} is the final state QCD corrections (1 for leptons), v_f is the vector, and a_f is the axial vector couplings of the final state to the Z^0. Table 1 gives the values of v, a and Γ for all possible final states. We do not include the contribution of the top quark in the computation of the total width. The limit on the top quark mass is currently greater than 60 GeV. Therefore the Z^0 cannot decay into a $t\bar{t}$ final state.

We compare the total measured width of the Z^0 to the expected value shown above. If the two are not consistent, then we know that the current Standard Model of the electroweak interaction is not complete. Such an inconsistency would only give a hint as to the new physics we are encountering.

We can measure the width by a variety of methods.[3,4] One way is to invoke e–μ–τ universality and therefore deduce that

$$\sigma_{e^+e^-\to\mu^+\mu^-} = \frac{12\pi}{m_Z^2 s} \frac{\Gamma_{\mu^+\mu^-}^2}{\Gamma_T} \quad . \tag{4}$$

Hence, measuring the cross section for $Z^0 \to \mu^+\mu^-$, and assuming that the Standard Model expression for $\Gamma_{\mu^+\mu^-}$ is valid determines Γ_T.

A second measure of the Z^0 width is the *invisible width*. The invisible width is the total width minus the width into all visible states. We again invoke lepton universality and find

$$\Gamma_{invisible} = \Gamma_T - 3\Gamma_{\mu^+\mu^-} - \Gamma_{hadrons} \quad . \tag{5}$$

We measure the width into hadrons by measuring the hadronic cross section for the Z^0 and then using the method described above to determine the total width.

Finally, we can measure the width of the Z^0 by scanning the beam energy and fitting the resulting line shape to the theoretically expected function.[5] Table 2 summarizes[3] the expected error in the measurement of the Z^0 width as a function of number of Z^0 events collected. The reader should note that the measurement of the invisible width has a smaller systematic error than the measurement of the total width due to a fortuitous cancellation of errors. Please see Ref. 3 for more details.

The mass of the Z^0 is related to the Weinberg angle and the Fermi coupling constant by

$$\frac{G_F(1-\Delta r)m_Z^2 s}{8\sqrt{2}\,\pi\alpha} = \frac{1}{16\sin^2\theta_w\cos^2\theta_w} \quad , \tag{6}$$

where Δr is the radiative correction to the ratio of the W to Z^0 masses squared $[(m_W/m_Z)^2]$. We can either fix Δr and use the measurement of Z^0 to determine $\sin^2\theta_w$ or we can use the measurement of $\sin^2\theta_w$ to determine Δr. We expect an error of 40 MeV on the mass of the Z^0 by measuring the energy of the beam pulse to pulse with the energy spectrometers.

We list the error on $\sin^2\theta_w$ and Δr as a function of the number of Z^0 events recorded in Table 3. We assume, for the purposes of this table, if we are determining $\sin^2\theta_w$, that $1-\Delta r$ is known to 0.01%. The value of $\sin^2\theta_w$ has been measured[6] to 2%. If we know Δr, we can measure $\sin^2\theta_w$ to 0.2% with 5000 events—an order-of-magnitude improvement in the error. However, the value of Δr depends strongly on the value of the mass of the top quark and weakly on the mass of the Higgs boson. The value of $1-\Delta r$ varies by 5% over the range of allowed masses of the top quark.[7,8] Therefore, the determination of the electroweak parameters is coupled to the top mass. Our measurement of the mass of the Z^0 will place an important constraint on the parameters of the Standard Model.

THE APPARATUS

The Mark II detector has been extensively described elsewhere.[9] A diagram of the detector is shown in Fig. 1.

We use the Mark II detector to record Z^0 and Bhabha events. The energies of both the positron and electron beams is determined by the energy spectrometers and is recorded with each candidate event. The visible final states of Z^0 decay are e^+e^-, $\mu^+\mu^-$, $\tau^+\tau^-$, or hadrons. All of these final states can be detected with the Mark II's combination of drift chambers, time of flight measurements, liquid argon and gas calorimetry and muon detection. We will concentrate on the determination of the collision energy.

The beam of electrons or positrons is kicked into its own extraction line after the interaction. We cause the beam to emit a swath of synchrotron light by a bending magnet. We then bend the beam in a plane perpendicular to the initial bend by a well-measured and -monitored spectrometer magnet. Finally, we cause the beam to emit a second swath of light in the same manner as the first. A schematic diagram of the optics of the extraction line are shown in Fig. 2.

The beam energy can be expressed as

$$E\,(\mathrm{GeV}) \;=\; 2.99792\,\frac{\int B\,dl}{\Delta\theta} \quad , \qquad \Delta\theta \;=\; \frac{d}{L} \quad , \tag{7}$$

where $\int B\,dl$ is the path integral of the magnetic field within the spectrometer magnet in tesla-meters, d is the distance between the two synchrotron radiation stripes, and L is the distance from the spectrometer magnet to the detectors of the light.

We use a television camera focused on a phosphorescent screen as our detector, as shown in Fig. 3(a). The video image is recorded and digitized for readout by a waveform recorder and a signal averager. A second detector is currently being installed; it detects synchrotron radiation through the ejection of electrons from

Cu-Be wires due to Compton scattering. A diagram of this detector is shown in Fig. 3(b).

We show an example of the light stripes digitized by the PSM in Fig. 4. The light stripes are quite visible over the background. The data analysis routine fits a Gaussian to each stripe. Each beam line has two stripes associated with it; one stripe from before the spectrometer magnet, the other after. Our analysis routine subtracts the distance between the two stripes to determine d for each beam line.

The data is digitized from the PSM each beam pulse. If the Mark II has a valid trigger, the data is recorded onto tape and analyzed both online and offline via the same routines. Figure 5 shows the energy determined on 100 consecutive Mark II triggers. The sigma of the measured energies is 5 MeV. This must be looked on as an upper limit for the short-term variations in the analysis algorithm since any jitter in the accelerator will be reflected in the histogram. We shall see that the other systematic errors on the measurement of the beam energy amount to about 20 MeV. The statistical error on the measurement of the beam energy is the energy spread of the beam divided by the square root of the number of Z^0 events collected. The energy spread of the beam is about 150 MeV. Therefore, with modest statistics (of order 5000 events), the measurement of the mass of the Z^0 is limited by the systematic error on the beam energy measurement.

SYSTEMATIC ERRORS

The systematic errors for this device are on the measurements of $\int B\,dl$, d, and L. The next sections describe each measurement separately.

The Field Integral ($\int B\,dl$)

We measured $\int B\,dl$ two ways in the laboratory and monitor it three ways online.[10] We measured $\int B\,dl$ by a "moving" wire and a "moving" probe in the laboratory and we monitor it online with a "flip" coil rotating at 3 rpm, an NMR probe and a current transducer. The spectrometer magnet in each beam line is monitored separately and the information from each is recorded event by event.

The "moving" wire measurement was done by passing a group of wires through the gap and returning them outside the magnet. This closed loop was then moved a precisely known distance, 10 mm. The induced voltage was recorded and $\int B\, dl$ determined by integrating the voltage in time (the emf). The measurement of $\int B\, dl$ is good to 40 parts per million (ppm) by this technique.[10,11]

The "moving" probe measurement was done by stepping a Hall and NMR probes through the magnet gap. The two probes determined the magnetic field at each point in the gap. The NMR was used in the region of uniform magnetic field, while the Hall probe measurement was used in the areas of the fringe field of the magnet. The NMR is, in general, much more accurate than the Hall probe, but in the fringe fields the NMR probe does not operate. We used a laser interferometer to determine the position of the probes. The accuracy of this measurement technique is 53 ppm.[12].

The values of the two techniques agreed to within 80 ppm, giving a total uncertainty in the $\int B\, dl$ of about 0.01%, which was our goal.

The "flip" coil we use for online monitoring of the magnetic field is simply a wire wrapped around and epoxied to a quartz rod. We also place an NMR probe with this assembly. Both devices are placed inside the magnetic gap but outside of the radiation zone of the beams. Both devices were cross-calibrated in the laboratory with the "moving" wire and "moving" probe measurements.

The "flip" coil and the NMR probe gave measurements with a mean difference of about 40 ppm over several months of running. We also observed magnetic field drifts of order 100 ppm over this time. This met our goal for accuracy of the $\int B\, dl$ measurement.

The Displacement Distance Measurement (d)

It is crucial that we know the physical position of the synchrotron stripe. We use a fiducial "bar" code to determine the exact position of the stripe. We strung a wire across the bottom of the screen. We allow a 1000-micron gap; then two wires

are strung with a 500 μm gap between them. We then string a group of three wires 1000 μm away from the group of two wires. The three wires are placed 500 μm apart. We continue this pattern until we achieve a group of eight wires. A group of 11 wires is strung at the top of the screen. The purpose of the wires is to cast a shadow onto the screen when we shine a strong light at the detector.

Figure 6 shows an example of the digitized reading from the PSM when we shine a light onto the detector. The dips correspond to the wires and the high pulse height are areas of the 1000 μm gaps. We calibrate the detector every eight hours by shining a light onto the detector and forming a correlation function to determine the absolute wire number each dip corresponds to.

We record the pixel position by using the three points near the minimum to determine a parabola. Figure 7 shows the stability of the difference between two adjacent wires in pixels over a one month period. We are stable to between 0.1 and 0.25 pixels, depending on the screen. This difference corresponds from 7 to 14 μm.

A survey of the wire positions was made in the laboratory. The wires were located to within 8 μm. We determined this error by using two methods to determine the wire position and repeating each method twice. We determine the position of the synchrotron light stripe by interpolating between the two wires that bracket the peak. The laboratory survey positions of the wire are then used to convert the pixel location into an absolute distance.

The distance between the two beams was about 27 cm. Therefore, adding the calibration error to the positioning error in quadrature, we determined that the systematic error in determining d was in the range of 40 to 60 ppm.

The Distance from the Magnet to the Screen (L)

The distance L results from a survey *in situ* of the apparatus. The data to determine this number to 100 ppm exists but has not yet been analyzed. We conservatively place an error of 0.1% on L currently.

Other Errors

We have several other sources of error. The first is that the synchrotron stripes are not parallel. We measured about a 1.5 mrad rotation of the top stripe relative to the bottom stripe, using the PSM. We estimate that this error contributes about a 40 ppm[12] uncertainty to the measurement of the beam energy. The most serious error is the systematic difference between the measured energy in the extraction line and the center of mass of the collision. If there is any residual dispersion at the IP, there could be a shift between the energy we measure in the extraction line and the energy at the IP. We conservatively estimate this error to be 30 MeV.[13] However, it is possible with increased understanding of the SLC, this error will decrease.

CONCLUSIONS

Combining all the estimated systematic errors for the extraction line spectrometers, we expect that the energy of each beam can be measured to 20 MeV.[13] The possible systematic shift between the center-of-mass energy and the energy measured in the extraction lines is about 30 MeV. Therefore, combining these errors in quadrature, we expect to measure the mass of the Z^0 to within 40 MeV. It is possible that the systematic study of $\mu^+\mu^-$ pairs will reduce the uncertainty in the energy shift between the IP and the beam energy measurement, but only with a large sample of events can this study even be attempted.

ACKNOWLEDGMENTS

The authors wish to thank the people who made the energy spectrometers possible. They include Tony Bell, Donald D. Briggs, William Brunk, Joe Cobb, Bernie Denton, Anne Hogan, Dave Jenson, Dan Jones, Ed Keyser, Michael Lateur, Jussi Oijala, Mark Petree, William Rowe, Martin Terman, John E. Tinsman, Dieter Walz and David Wilkinson.

REFERENCES

1. *cf.* COMMINS, E. D. & P. H. BUCKSBAUM. 1983. Weak interactions of leptons and quarks. Cambridge University Press, Cambridge, England; HALZEN, F. & A. D. MARTIN. 1984. Quarks and leptons: an introductory course in modern particle physics. John Wiley and Sons, New York.

2. RANKIN, P. 1987. Z^0 measurements: the theory and the practice. Proceedings of the Third MARK II Workshop on SLC Physics. SLAC–Report–315:63–98.

3. FELDMAN, G. 1987. On the possibility of measuring the number of neutrino species to a precision of 1/2 species with only 2000 Z events. *Ibid.:* 169–171.

4. FELDMAN, G. 1987. Measurement of the total hadronic cross section. *Ibid.:* 165–167.

5. ALEXANDER, J. *et al.* Measurement of the total hadronic cross section. *Ibid.:* 116–152.

6. The Particle Data Group, AGUILAR-BENITEZ, M. *et al.* 1988. Review of particle properties. Phys. Lett. **B204.**

7. MARCIANO, W. J. 1987. Weak neutral currents and the future Z mass measurements (anticipating SLC). Proceedings of the 15th SLAC Summer Institute on Particle Physics. SLAC–Report–328:645.

8. MARCIANO, W. J. 1986. $sin^2\theta_w$ and radiative corrections. Proceedings of the XXIII International Conference on High Energy Physics. Vol. II:999. World Scientific.

9. ABRAMS, G. *et al.* 1989. The Mark II detector for the SLC. SLAC–PUB–4558. Submitted to Nucl. Instr. Methods.

10. WATSON, S. *et al.* 1989. Precision measurements of the SLC reference magnets. SLAC–PUB–4908. Presented at the IEEE Particle Accelerator Conference, Chicago, IL, March 20–23, 1989.

11. LEVI, M. *et al.* 1989. Precision measurements of the SLC spectrometer magnets. SLAC–PUB–4654. Submitted to Nucl. Instr. Methods A.

12. LEVI, M. *et al.* 1989. Phosphorescent monitor for the SLC beam energy. SLAC–PUB–4921. Presented at the IEEE Particle Accelerator Conference, Chicago, IL, March 20–23, 1989.

13. KENT, J. *et al.* 1989. Precision measurements of the SLC beam energy. SLAC–PUB–4922. Presented at the IEEE Particle Accelerator Conference, Chicago, IL, March 20–23, 1989.

Table 1: Width of Z^0 into final states. We assume[2]: $\sin^2\theta_w = 0.222$, $Z^0 = 93$ GeV, and $\alpha_s = 0.13$. Note that ν and e refer to e, μ and τ; u refers to u and c quarks; d refers to d, s and b quarks.

f	v	a	Γ (MeV)
ν	1	1	176
e	$-1+4\sin^2\theta_w$	-1	89
u	$1-\frac{8}{3}\sin^2\theta_w$	1	321
d	$-1+\frac{4}{3}\sin^2\theta_w$	-1	412
all			2673

Table 2: Expected error on width measurement.

N_Z	$\Delta\Gamma_T$ (MeV)	$\Delta\Gamma_{invisible}$ (MeV)	$\Delta\Gamma_T$ scan (MeV)
500	215	142	248
1000	156	105	175
2000	115	81	124
5000	82	62	78
10000	67	54	55

Table 3: Expected errors on $\sin^2\theta_w$ and $1-\Delta r$, if we fix Δ_r or $\sin^2\theta_w$, respectively.

N_Z	$\delta\sin^2\theta_w$	$\delta(1-\Delta r)$
500	0.0008	0.033
5000	0.0004	0.033
10000	0.00036	0.033

FIGURE CAPTIONS

Figure 1: A diagram of the Mark II detector at the SLC.

Figure 2: Schematic diagram of extraction line optics.

Figure 3: (a) Diagram of the phosphorescent screen monitor (PSM). (b) Diagram of the secondary emission detector, the Wire Imaging Synchrotron Radiation Detector (WISRD).

Figure 4: Examples of digitized synchrotron light stripes from the PSM.

Figure 5: Energy determined for 100 consecutive pulses.

Figure 6: The shadowing of the wires strung over the wire frame holding the phosphorescent screen. The dips correspond to wires and the large pulse heights to 1000 μm gaps.

Figure 7: The stability of the difference between two consecutive wires in pixels for each of the four PSM screens.

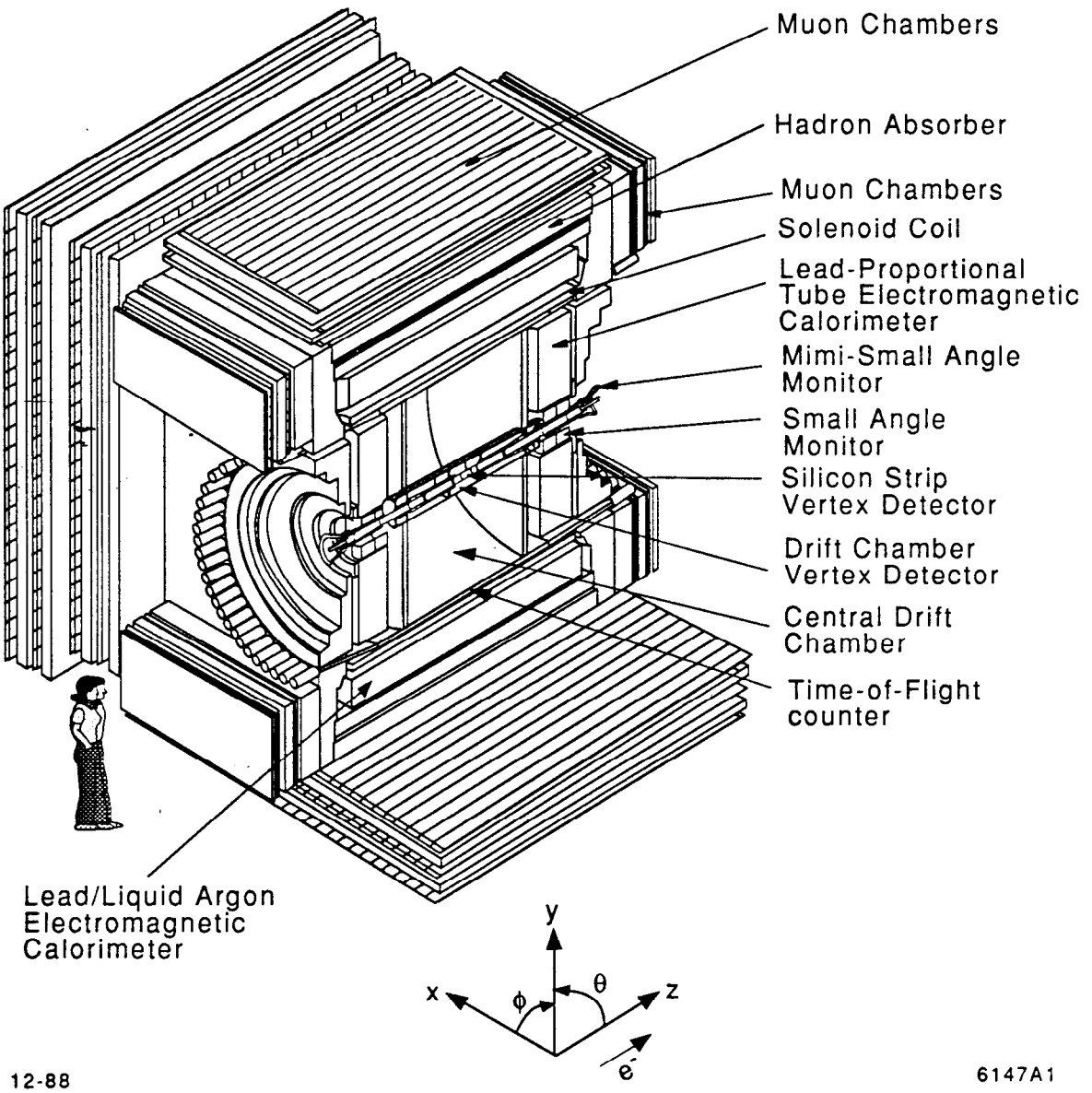
MARK II AT SLC
Muon Chambers
Hadron Absorber
Muon Chambers
Solenoid Coil
Lead-Proportional Tube Electromagnetic Calorimeter
Mimi-Small Angle Monitor
Small Angle Monitor
Silicon Strip Vertex Detector
Drift Chamber Vertex Detector
Central Drift Chamber
Time-of-Flight counter
Lead/Liquid Argon Electromagnetic Calorimeter
y
x
z
θ
φ
e⁻
12-88
6147A1

Fig. 1

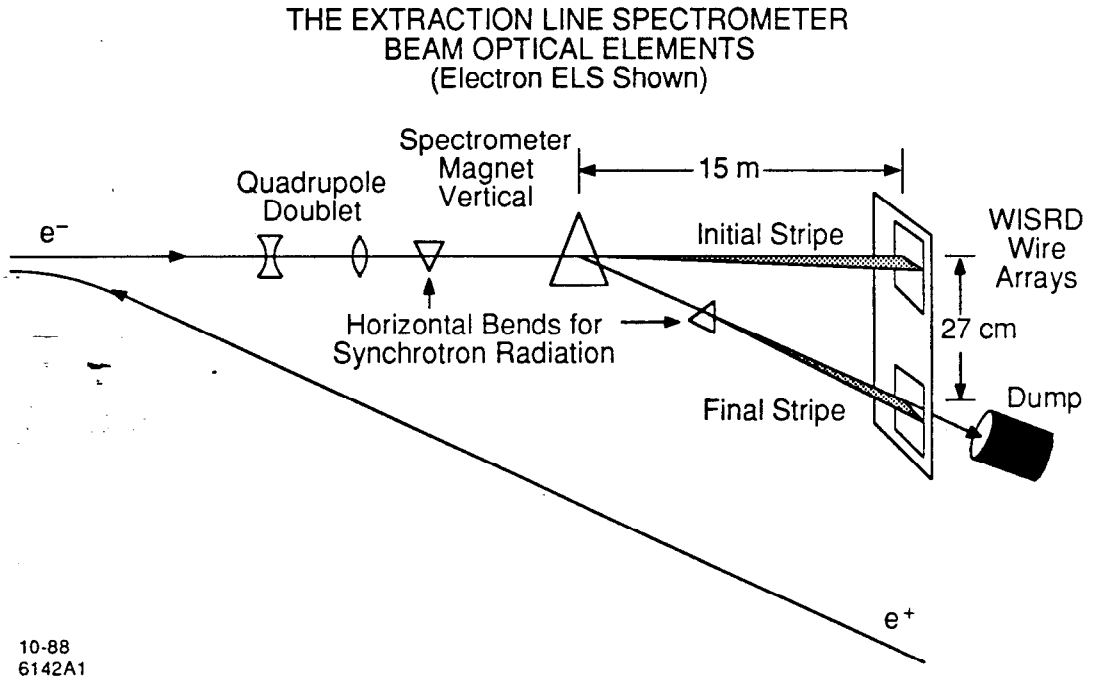
THE EXTRACTION LINE SPECTROMETER
BEAM OPTICAL ELEMENTS
(Electron ELS Shown)
Spectrometer
Magnet
Vertical
15 m
Quadrupole
Doublet
e⁻
Initial Stripe
WISRD
Wire
Arrays
27 cm
Horizontal Bends for
Synchrotron Radiation
Final Stripe
Dump
e⁺
10-88
6142A1

Fig. 2

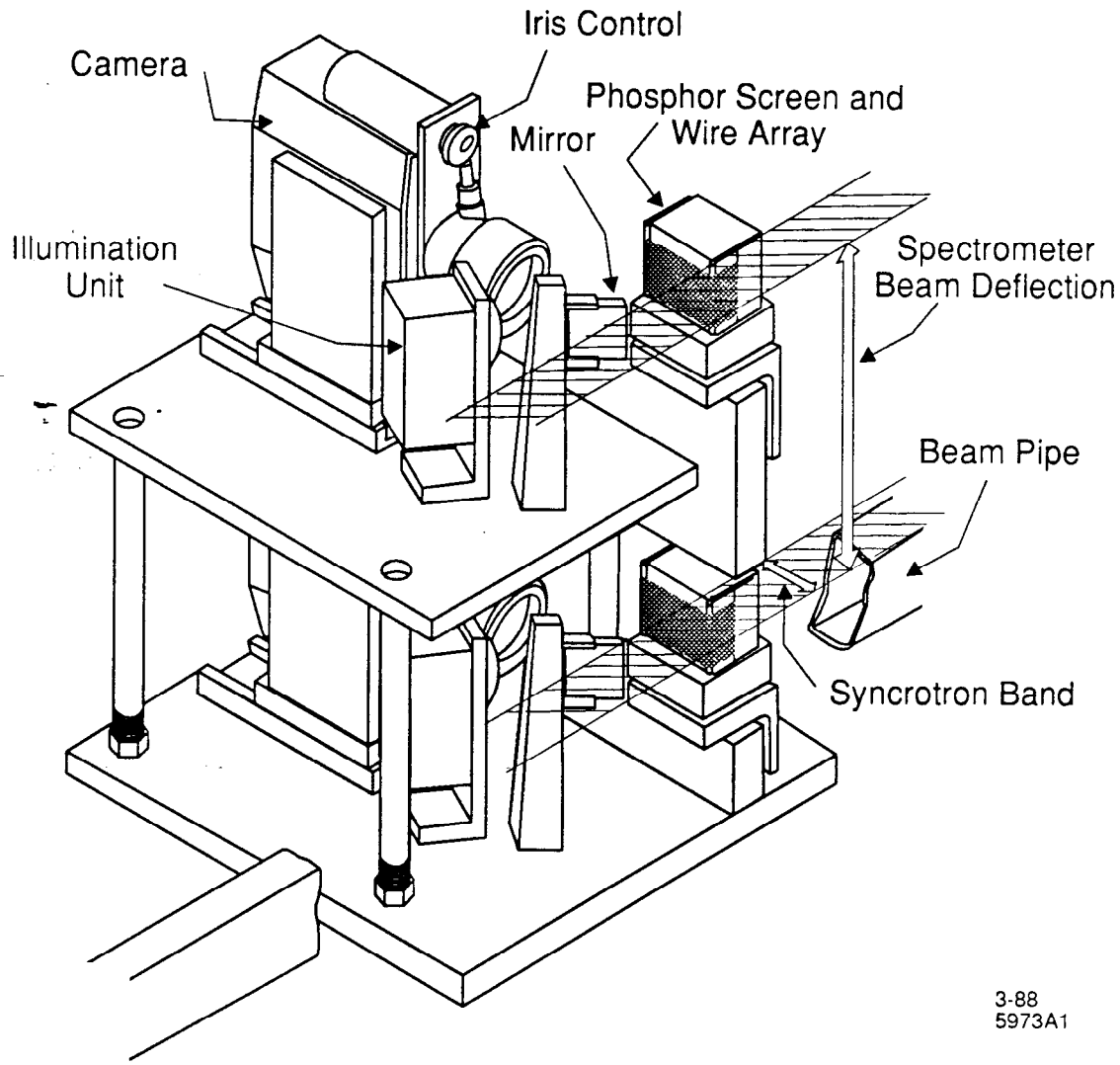
Iris Control
Camera
Phosphor Screen and
Wire Array
Mirror
Illumination
Unit
Spectrometer
Beam Deflection
Beam Pipe
Syncrotron Band
3-88
5973A1

Fig. 3a

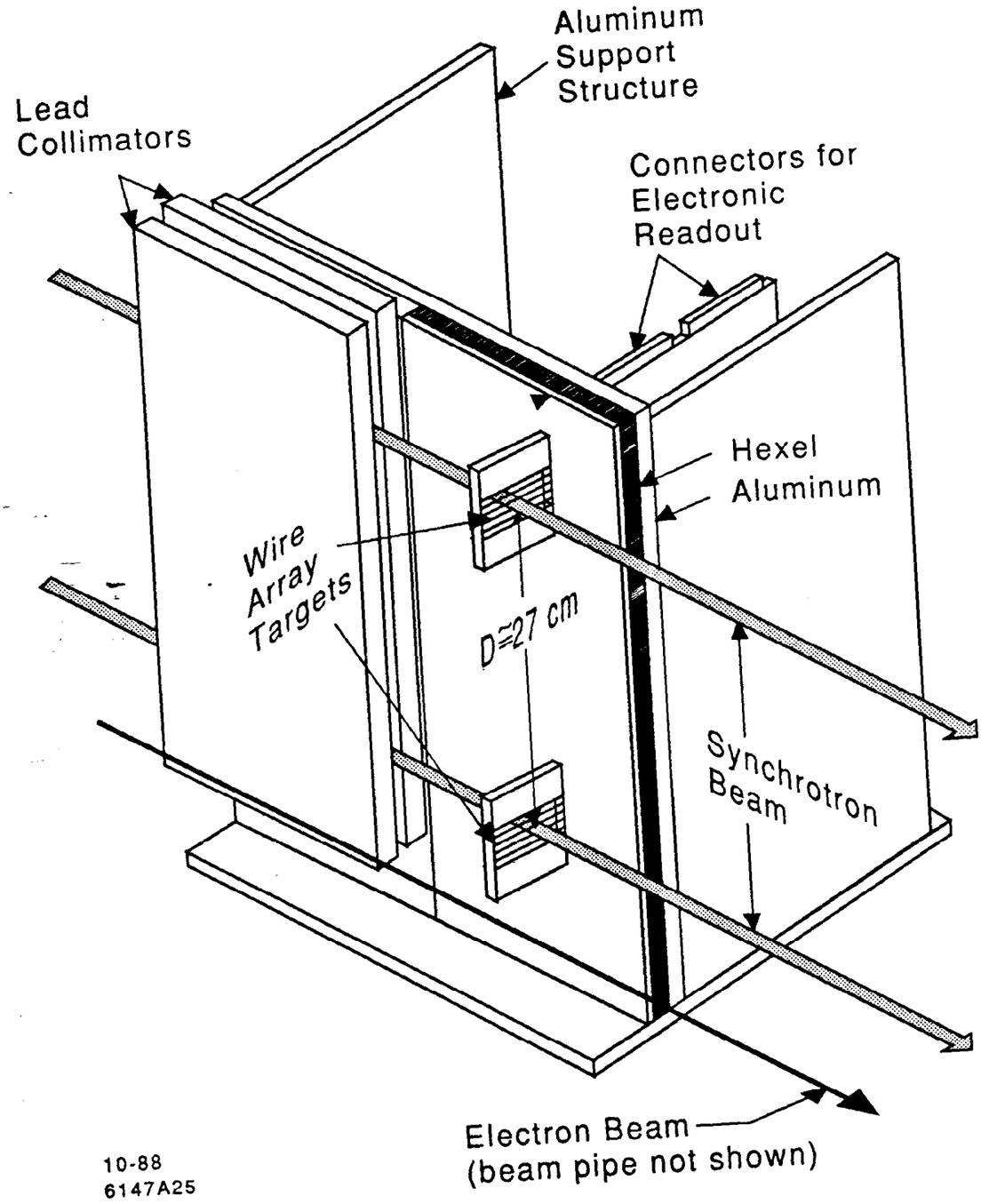
Aluminum
Support
Structure
Lead
Collimators
Connectors for
Electronic
Readout
Hexel
Aluminum
Wire
Array
Targets
D≈27 cm
Synchrotron
Beam
Electron Beam
(beam pipe not shown)
10-88
6147A25

Fig. 3b

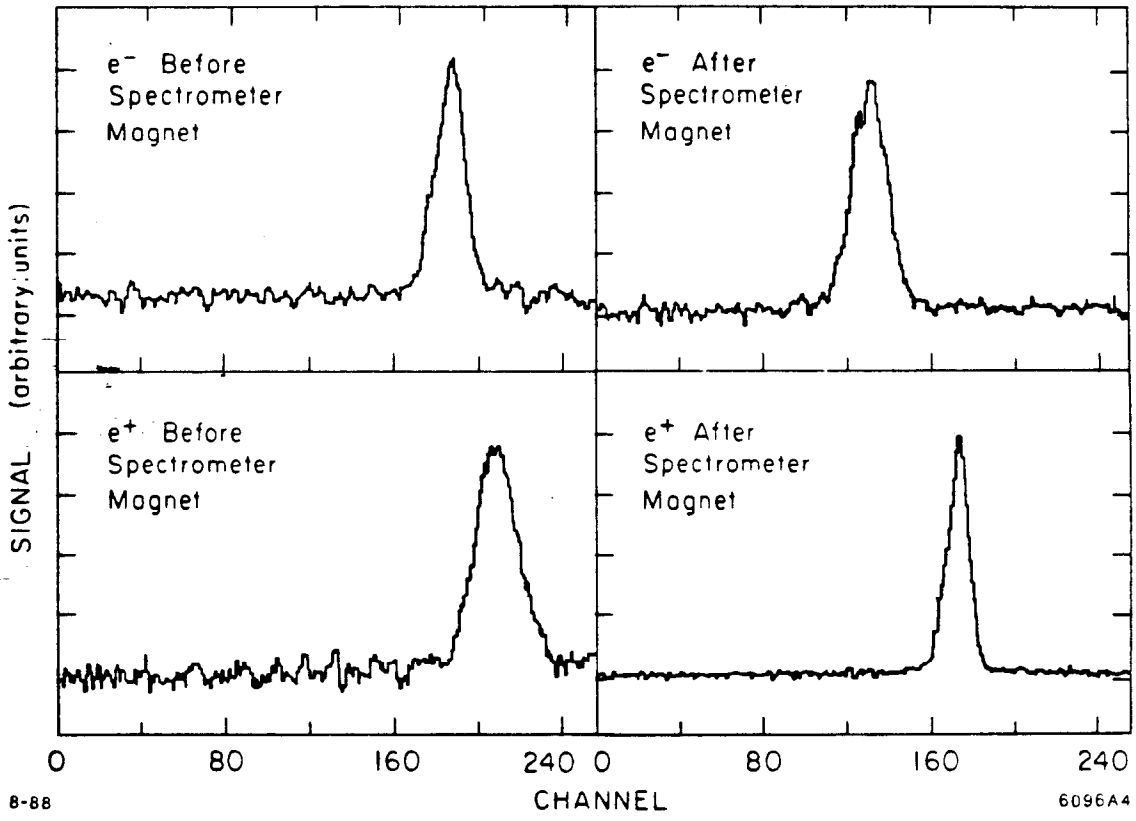
e⁻ Before Spectrometer Magnet
e⁻ After Spectrometer Magnet
e⁺ Before Spectrometer Magnet
e⁺ After Spectrometer Magnet
SIGNAL (arbitrary units)
0
80
160
240
0
80
160
240
CHANNEL
8-88
6096A4

Fig. 4

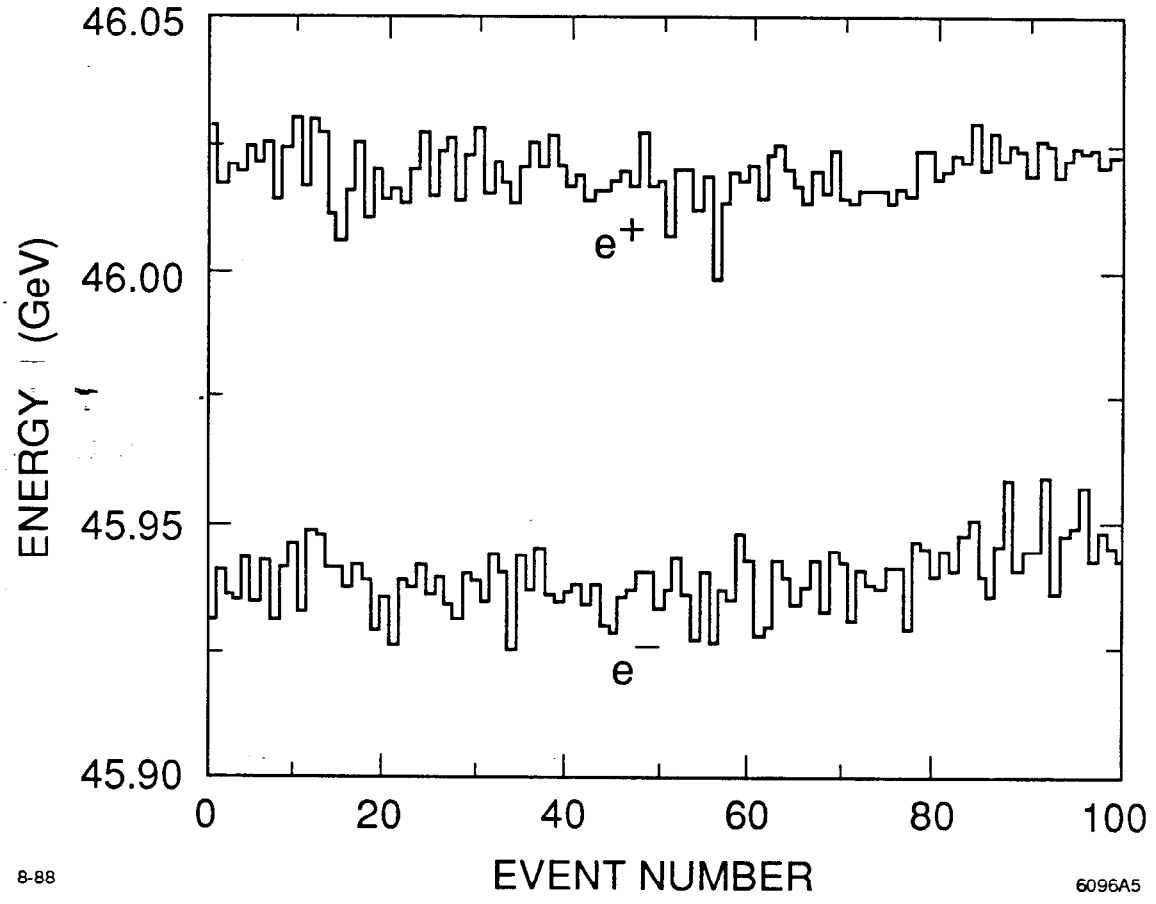
46.05
46.00
45.95
45.90
ENERGY (GeV)
e+
e−
0
20
40
60
80
100
EVENT NUMBER
8-88
6096A5

Fig. 5

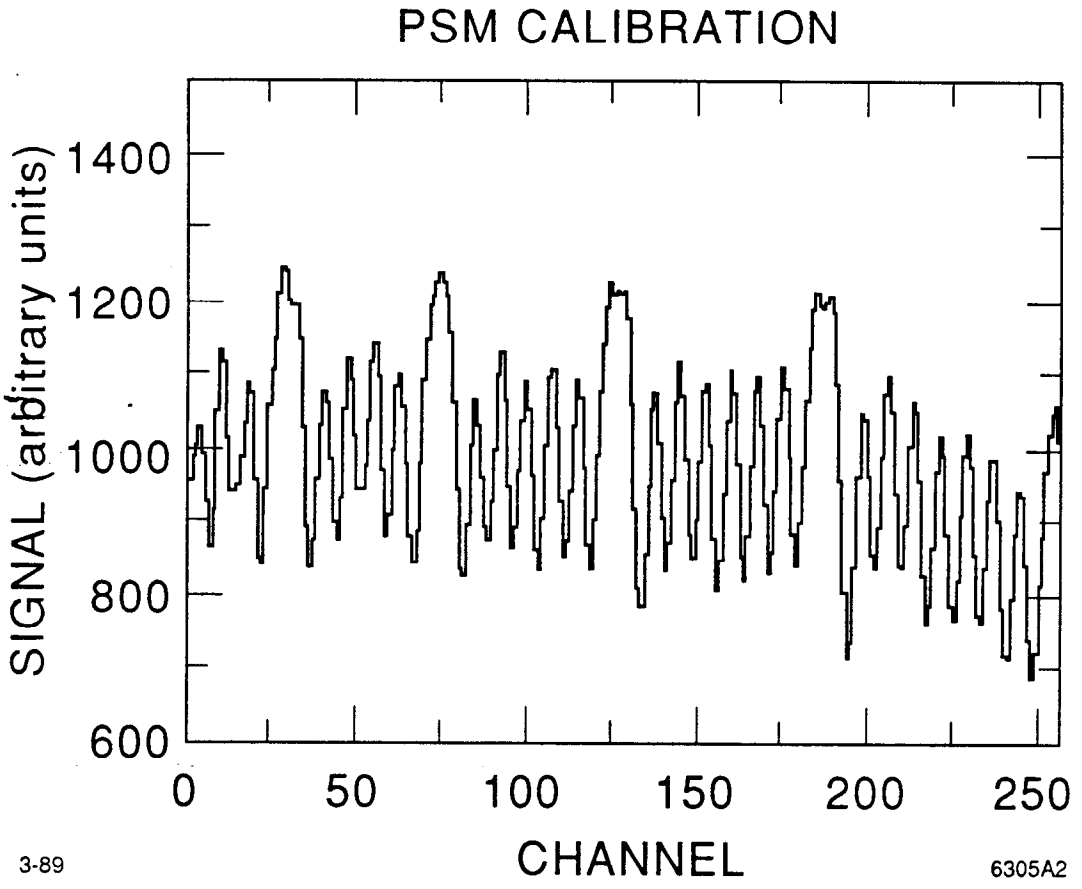
PSM CALIBRATION
SIGNAL (arbitrary units)
1400
1200
1000
800
600
0
50
100
150
200
250
CHANNEL
3-89
6305A2

Fig. 6

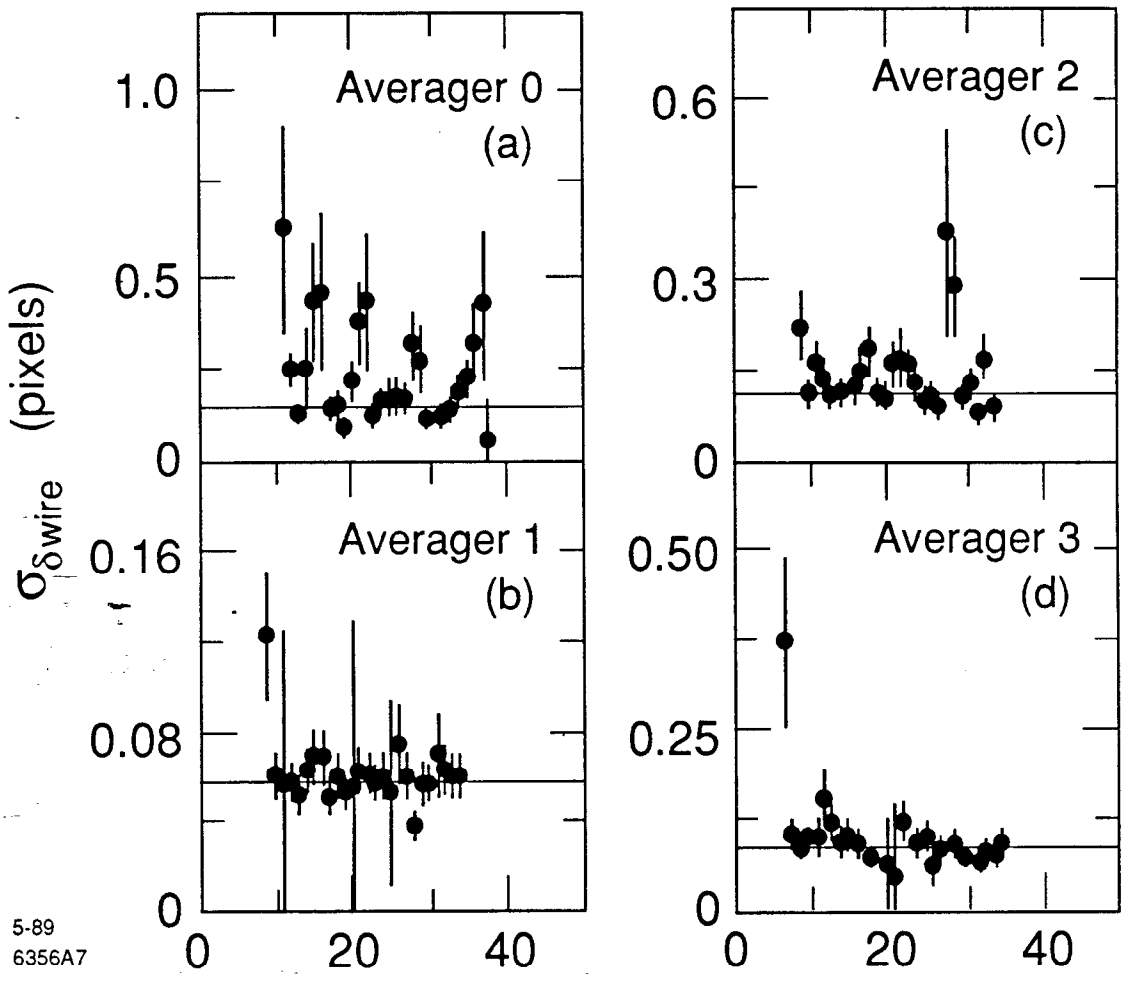
Averager 0
(a)
Averager 1
(b)
Averager 2
(c)
Averager 3
(d)
$\sigma_{\delta wire}$ (pixels)
1.0
0.5
0
0.16
0.08
0
0.6
0.3
0
0.50
0.25
0
0
20
40
0
20
40
5-89
6356A7

Fig. 7